

Restoration of Large Damage Volumes in Polymers

S. R. White,^{1,2*} J. S. Moore,^{2,3} N. R. Sottos,^{2,4} B. P. Krull,^{2,4} W. A. Santa Cruz,^{2,3} R. C. R. Gergely^{2,5}

The regenerative power of tissues and organs in biology has no analog in synthetic materials. Although self-healing of microscopic defects has been demonstrated, the regrowth of material lost through catastrophic damage requires a regenerative-like approach. We demonstrate a vascular synthetic system that restores mechanical performance in response to large-scale damage. Gap-filling scaffolds are created through a two-stage polymer chemistry that initially forms a shape-conforming dynamic gel but later polymerizes to a solid structural polymer with robust mechanical properties. Through the control of reaction kinetics and vascular delivery rate, we filled impacted regions that exceed 35 mm in diameter within 20 min and restored mechanical function within 3 hours. After restoration of impact damage, 62% of the total absorbed energy was recovered in comparison with that in initial impact tests.

Whereas biology achieves regeneration through vascularization and recruitment of stem cells (1–3), engineering materials are generally avascular, with a limited ability to self-heal (4, 5). A variety of repair strategies exist for microscopic defects and cracks (6–10), but autonomic restoration of materials that suffer large-scale damage and associated mass loss has not been realized. Restoration requires overcoming the interplay of mass transport, environmental factors, intrinsic forces (such as surface tension), and extrinsic forces (such as gravity) that act on liquid reagents and the chemical reactions associated with damage repair.

Our restoration concept for structural materials is illustrated in Fig. 1. The strategy is predicated on the delivery of reactive fluids through two independent vascular networks to the site of damage. Events that lead to substantial mass loss (such as ballistic impact) trigger release of fluids, subsequent mixing, and initiation of the restoration process. A reactive system that progresses from liquid to gel (gel stage) and gel to polymer (polymer stage) is hypothesized to deliver low-viscosity fluids to the site of damage, initially resulting in a shape-conforming yet self-supporting viscoelastic scaffold. Addition of new material proceeds until the damaged region is fully filled and complete replacement of lost mass is achieved. Transformation of the gel into a stiff polymer then allows for recovery of the mechanical properties of the original material.

We developed a two-stage polymer chemistry in which catalyzed gelation of liquid monomer is followed by bulk polymerization to a structural solid (Fig. 1). The reactive monomer solutions begin as stable, low-viscosity (time t_0), until damage-triggered release initiates the chemical

processes. A relatively fast gel stage (time t_1 , from 30 s to a few minutes) creates a semisolid scaffold on which additional solution is accreted. Gelators A, a bis-acylhydrazine-terminated poly(ethylene glycol), and B, a tris[(4-formylphenoxy)methyl]ethane, form a cross-linked network of dynamic acylhydrazone bonds through acid-catalyzed condensation (synthesis is provided in fig. S1) (11). This chemistry is capable of gelling a wide range of organic liquids, including acrylic and thiol-ene monomers. Monomer gelation accomplishes the need to fill gaps stemming from mass loss, and conversion to polymer completes the restoration process. Polymerization kinetics on a time scale $> t_1$ (hours) avoids premature stiffening of the restored material. Room-temperature polymerization is achieved with judicious choice of radical initiators, promoters, and inhibitors. Although biological systems require a complex and highly regulated system of biochemical processes to achieve regeneration (12–19), our strat-

egy produces reliable performance with relatively simple synthetic reagents.

The properties of the structural polymer are tailored by selection of the monomer, as demonstrated below with two examples. In one example, a thermoplastic was polymerized by using 2-hydroxyethyl methacrylate (HEMA) initiated by a radical redox reaction between methyl ethyl ketone peroxide (MEKP) initiator and cobalt naphthenate (CoNp) promoter (20); in a second example, liquid thiol-ene agents 1,3-glyceryl dimethacrylate and trimethylolpropane tris(3-mercaptopropionate) react to form a thermosetting material (fig. S2). Monomers were selected to fulfill a stringent set of requirements, including high boiling point, nonwetting properties, low viscosity, favorable cure kinetics, and the ability to dissolve gelators. The reagents required for each example are mutually compatible with the reagents for gelation chemistry. Independently tunable chemical triggers selectively control the rates of both gelation and polymerization. The components for both examples are strategically divided into two stable solutions and loaded into separate microchannels (Fig. 1, left, and table S6).

Oscillatory rheology confirmed the separate occurrence of gelation and polymerization stages as well as the ability to regulate the reaction kinetics of each stage (Fig. 2, A to C). A representative reaction shown in Fig. 2A shows the evolution of storage (G') and loss (G'') moduli of a 12 weight percent (wt %) gelator solution in HEMA. The first plateau of G' reflects monomer gelation to a $\sim 10^4$ to 10^5 Pa semi-solid. Onset of the gel stage (t_1) was defined as the crossover of G' and G'' . The second modulus plateau, several orders of magnitude higher, reflects a slower transformation from gel to structural polymer.

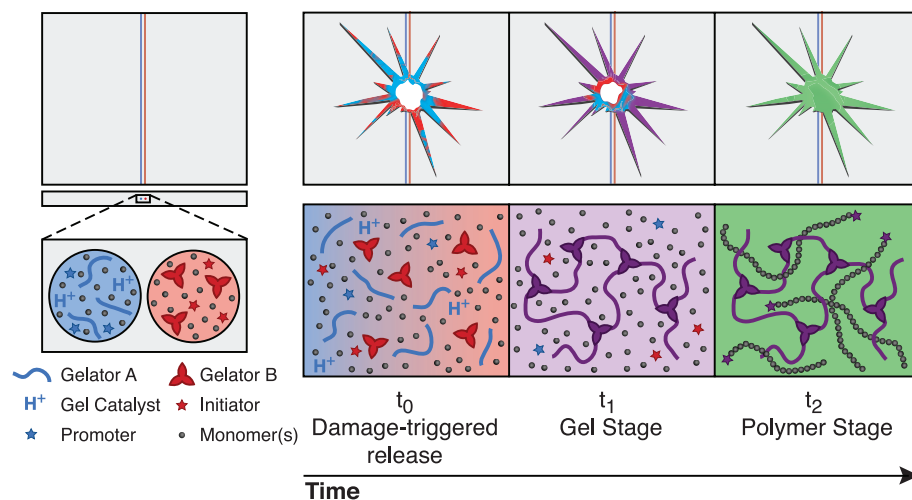


Fig. 1. Two-stage restoration strategy. Reactive monomer solutions are incorporated into a vascularized specimen (blue and red channels). Time t_0 , impact damage initiates fluid release into the damage region. Time t_1 , gel stage (purple) occurs by covalent cross-linking of gelators A and B with an acid catalyst. Deposition of fluid and subsequent gelation continues until the void is filled. Time t_2 , the polymer stage (green) follows by using a two-component initiation for monomer polymerization, resulting in recovery of structural performance. Chemical structures of the two-stage polymer system are given in fig. S2.

¹Department of Aerospace Engineering, University of Illinois at Urbana-Champaign, Urbana, IL 61801, USA. ²The Beckman Institute, University of Illinois at Urbana-Champaign, Urbana, IL 61801, USA. ³Department of Chemistry, University of Illinois at Urbana-Champaign, Urbana, IL 61801, USA. ⁴Department of Materials Science and Engineering, University of Illinois at Urbana-Champaign, Urbana, IL 61801, USA. ⁵Department of Mechanical Science and Engineering, University of Illinois at Urbana-Champaign, Urbana, IL 61801, USA.

*Corresponding author. E-mail: swhite@illinois.edu

Polymerization onset (t_2) was designated as the peak of the loss factor ($\tan \delta = G''/G'$) (fig. S3A). Rates of gelation and polymerization are largely independent (fig. S4), which enables precise control of t_1 and t_2 by varying the concentrations of catalyst for the gelation reaction and initiators for the polymerization reaction. Plots of the time scales of staged transitions for the HEMA example are shown in Fig. 2, B and C. Gelation rate is dependent on catalyst concentration and determines the scaffold-forming ability (Fig. 2B). Control of polymerization was achieved by varying promoter concentration in an inert environment (Fig. 2C). However, free-radical polymerizations of acrylates are sensitive to atmospheric oxygen. In contrast, the thiol-ene thermoset chemistry is oxygen-tolerant and cures in aerobic environments. Thiol-ene polymerizations are fast and have been known to cure without the use of initiators (21). To allow sufficient time for gel formation, the radical inhibitor cupferron was used to slow the polymerization rate (fig. S3B) (22, 23). The ability to tune the rates of our two-stage restorative system enables adaptation to a wide variety of damage geometries.

Gelation allows deposition of material beyond that which is dictated by surface tension alone. When damage size exceeds a certain threshold, surface tension is insufficient to retain unreacted fluid, and gravity pulls it out of the damage zone. The boundary between surface tension and gravity-dominated regimes (described by Tate's Law and the drop-weight method of analysis) (fig. S5) (24–26) was validated for our experimental setup with standard test fluids (Fig. 2D). In contrast to these nonreactive fluids, the gel deposition volume exceeds that expected from Tate's Law by over an order of magnitude. Two formulations con-

taining different gel fractions are plotted in Fig. 2D, with the greater gel fraction producing a larger deposition volume. The increase in volume retained over nonreactive fluids is due to the mechanical support of the in situ–formed gel. If gelation and deposition occur on the same time scale, the growing material is no longer retained by the surface tension of the fluid alone; it is also retained by the cohesion of the restored material and its adhesion to the deposition surface.

In our model experiments, the restorative reagents span gaps and fill large damage volumes by forming a free-standing, dynamic gel scaffold on which continued material growth occurs. We used an open cylinder (sample dimensions are 52 by 52 by 3 mm thick, 330- μ m-diameter parallel channels) (fig. S6A) as a model geometry to test the filling of large-scale damage in thin epoxy sheets. Solutions of HEMA-containing gelators, acid catalyst, and fluorescent dye (Nile Red and perylene) were delivered to the damage area via separate microchannels (Fig. 3A). A computer-controlled, pressurized system ensures reagents were delivered at 1:1 volume ratios (supplementary materials, materials and methods). Upon entering the damaged region, the components mix and quickly wet the inner surface of the sample owing to low viscosity and a low fluid-substrate contact angle (table S1). Rapid gelation forms a scaffold on which additional fluid from the microvascular channels was deposited. The faceted appearance of the recovering damage region (Fig. 3A) reflects the mechanical stiffness of the developing gel because an ideal liquid would assume a smooth circular shape to minimize surface energy. Gelled material grows inward, and the entire damage region is filled as the process of deposition and gelation continues. The dynamic nature

(27) of the gelator chemistry enables continuous (defect-free) gel interfaces and the formation of a monolithic plug in place of the original void.

Restoration to full mechanical function was accomplished by replenishing lost mass and transforming the gelled monomer to a fully polymerized solid. The filling performance of gelling and nongelling controls is compared for increasing damage area in Fig. 3B. The area fill ratio (AFR) is calculated for each damage area as the ratio $A_{\text{fill}}:A_0$, where A_{fill} is the area filled by the restorative solutions and A_0 is the total damage area. The control solutions achieve an AFR of 1 only for diameters up to 6.3 mm. For larger diameters, the effect of gravity dominates surface tension and causes the controls to drip out of the damaged region, which results in incomplete filling. In contrast, gelling solutions fill to capacity (AFR = 1) for damage diameters up to 9.0 mm by overcoming gravity and circumventing failure by dripping. Damage sizes exceeding 8.0 mm do not reliably fill for all replicates because gravity causes gel material to grow downward rather than toward the damage center; however, the AFR remains substantially higher than that of control solutions because of superior material retention.

A pressure cell was used to verify mechanical recovery of our system by applying 345 kPa of nitrogen to one side of a damage sample and monitoring leakage on the opposite side (fig. S6B) (28). Because only a completely filled damage region will withstand pressurization, we tested the maximum damage areas at which each restorative system attained complete filling for each of five replicates (Fig. 3C). All gelling systems are able to fill larger damage areas than can nongelling solutions but do not provide mechanical recovery without a second transition to polymer.

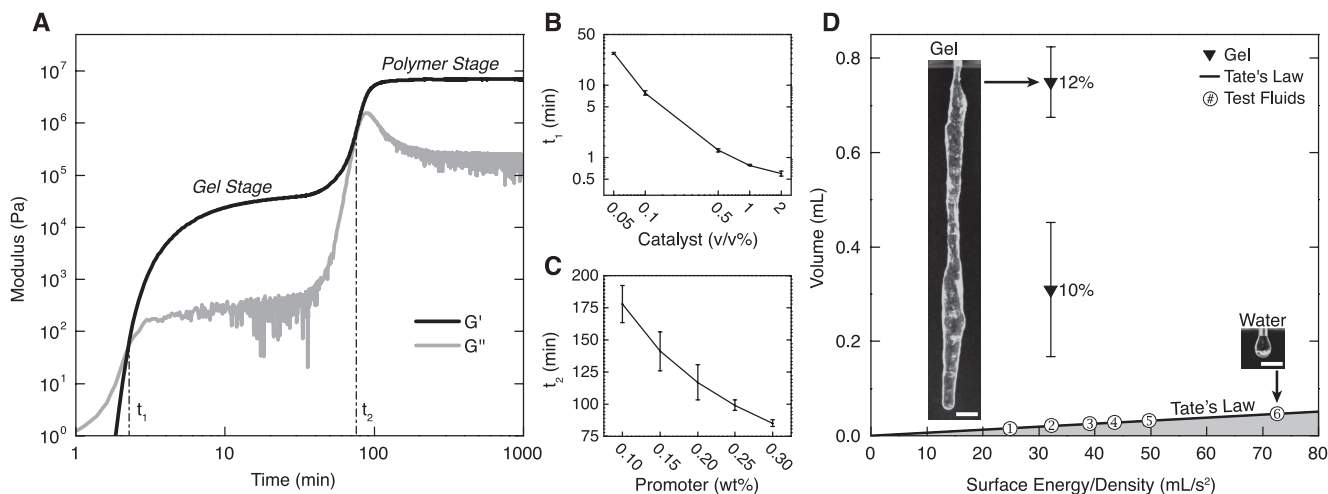


Fig. 2. Characterization of the two-stage process. Solutions contain gelators in HEMA (monomer) with dichloroacetic acid (catalyst), methyl ethyl ketone peroxide (initiator), and cobalt naphthenate (promoter). **(A)** Rheological properties of the restorative reagents over time display both the fast formation of the organogel (t_1 , seconds to minutes), and slower reaction rate to polymer (t_2 , hours) controlled by the concentrations of chemical triggers. **(B)** Control of gel-stage kinetics by varying catalyst concentration (1.5 wt % initiator, 0.1 wt % promoter). **(C)** Control of polymer stage kinetics by varying promoter (2 v/v % catalyst,

1.5 wt % initiator). **(D)** Volume deposited by using restorative gel chemistry (HEMA gel, 2 v/v % catalyst, no initiator or promoter). Tate's Law describes the limiting volume of a nonreactive fluid that can be retained with surface tension; standard test fluids confirm this relationship (1, pentane; 2, HEMA; 3, dimethyl sulfoxide; 4, ethylene glycol; 5, glycerol; and 6, water). Two-stage chemistry far exceeds this limit, but deposition is dependent on the concentration of gelators. The inset optical image on the left shows the volume deposited by 12 wt % gelators, whereas the inset optical image on the right shows water test fluid. Scale bars, 5 mm.

Only the thermoplastic and thermoset two-stage polymers combine filling performance with mechanical recovery. A standard two-part epoxy resin is presented for comparison, and neither fills a substantial damage area nor seals after a 24-hour room-temperature cure. As demonstrated with larger-area fill ratios and higher seal rates, two-stage polymers provide restoration perform-

ance superior to traditional healing chemistries (29). The final mechanical properties of the two-stage polymer systems are comparable with commercial poly(methyl methacrylate) (PMMA) polymers (30). Quasistatic tensile testing of the two-stage thermoplastic (HEMA) system yields an elastic modulus of 1.8 GPa and a tensile strength of 45 MPa (fig. S7 and table S2).

To test more realistic damage modes, we impacted and punctured specimens using a drop tower apparatus. The multiscale damage present in impact specimens represents a substantial challenge and requires chemistry that can both regrow the lost mass as well as penetrate into microcracks to create a pressure-tight seal. Dropping a striker with a hemispherically shaped tip at 6.26 J (Fig. 4A)

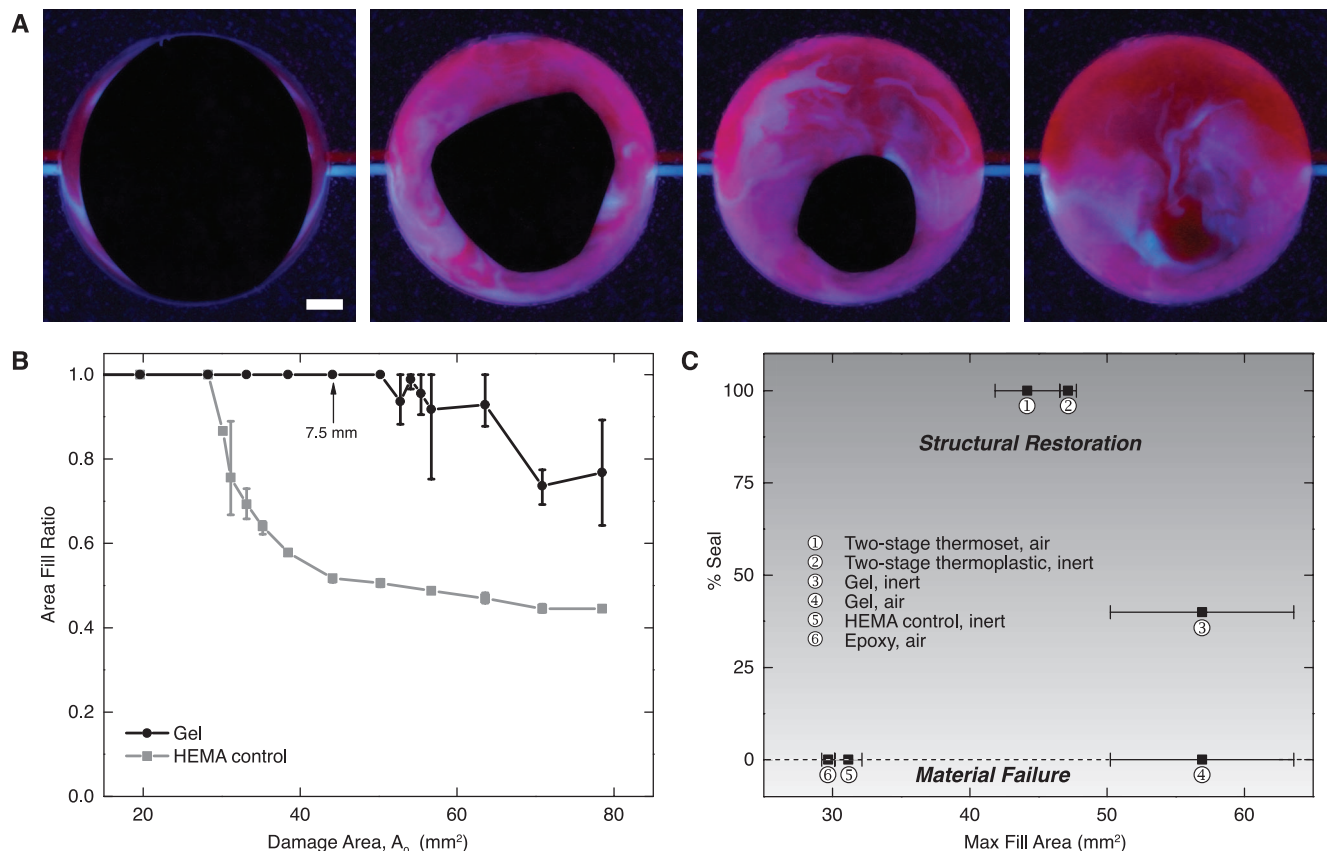


Fig. 3. Cylinder damage geometry to test restoration performance. (A) Optical images of 7.5-mm-diameter open-cylinder damage geometry after 1, 3, 7, and 13 min (left to right) pressurized delivery of HEMA gel solutions (2 v/v % catalyst, no initiator or promoter). Blue liquid is part A [HEMA, gelator A (56% of total gel A), DCA catalyst] dyed with perylene, and red liquid is part B [HEMA, gelator A (44% of total gel A), gelator B] dyed with Nile Red. Scale bar, 1 mm.

(B) Fill performance achieved for cylindrical holes of increasing size for HEMA gel and a nongelling neat HEMA control. $AFR = A_{\text{fill}}/A_0$. **(C)** Restoration performance of various healing systems after a 24-hour room-temperature cure, with the curing atmosphere indicated in the legend. Samples are subjected to 345 kPa N_2 pressure loading. Restoration requires both a complete fill and recovery of full mechanical function.

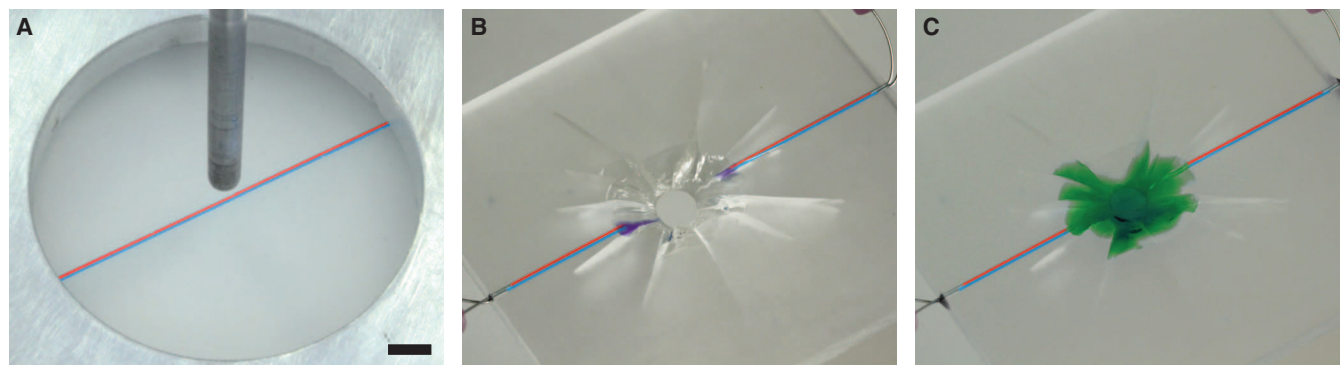


Fig. 4. Restoration of impact damage. Perspective views of impact specimen restored with two-stage thermoplastic (HEMA) system (0.1 v/v % catalyst, 1.5 wt % initiator, 0.1 wt % promoter). Both components of two-part solutions are dyed and recolored in images for visualization. **(A)** Specimen

mounted into impact test fixture; 4-mm striker with a hemispherically shaped tip suspended over specimen. **(B)** and **(C)** Impact damage with central puncture and radiating cracks **(B)** before filling and **(C)** after filling. Scale bar, 5 mm.

creates a central puncture and radiating cracks, with damage spanning ~35 mm in diameter. We implemented the same pressurized delivery scheme to fill the damage post-impact. A dye (Oil Blue N) was used to observe the deposition process, which included wicking into the radiating cracks (Fig. 4, B and C). Although fast gelation chemistry is advantageous for the regrowth of lost mass, it may not provide sufficient time for the reagents to fully penetrate into radiating microcracks. By tuning (slowing) the gelation kinetics, we were able to achieve gap-filling and partial penetration of radial microcracks emanating from the central hole. Pressure testing of impact samples yielded ~60% sealing success, with most failures attributed to the lack of sealing of the dense network of radiating microcracks. After restoration of impact damage, we reimpacted specimens using the same testing protocol and measured 62% recovery of total absorbed energy in comparison with the initial impact test. The restored material performed on par (76%) with control specimens in which the native substrate material was injected into the damage and cured at a high temperature (table S3).

We have demonstrated a vascular approach to damage restoration using a polymer that replaces lost mass and recovers structural performance. Our two-stage chemistry makes use of both a rapid gelation (gel stage) for gap-filling scaffolds and a slower polymerization (polymer stage) for restoration of structural performance. When damage is unpredictable and uncontrolled, more complex and interconnected vascular networks (31) will be necessary to provide sufficient vascular

coverage and redundancy to circumvent channel blockage. Truly regenerative polymers may be possible in the future via on-demand delivery of the chemical components of the native substrate polymer coupled with tunable gel and polymer transitions.

References and Notes

1. K. D. Birnbaum, A. Sánchez Alvarado, *Cell* **132**, 697–710 (2008).
2. M. D. C. Carnevali, F. Bonasoro, E. Lucca, M. C. Thorndyke, *J. Exp. Zool.* **272**, 464–474 (1995).
3. R. J. Lauzon, K. J. Ishizuka, I. L. Weissman, *Dev. Biol.* **249**, 333–348 (2002).
4. E. B. Murphy, F. Wudl, *Prog. Polym. Sci.* **35**, 223–251 (2010).
5. R. P. Wool, *Soft Matter* **4**, 400–418 (2008).
6. B. J. Blaiszik *et al.*, *Annu. Rev. Mater. Res.* **40**, 179–211 (2010).
7. X. Chen *et al.*, *Science* **295**, 1698–1702 (2002).
8. P. Cordier, F. Tournilhac, C. Soulié-Ziakovic, L. Leibler, *Nature* **451**, 977–980 (2008).
9. A. C. Balazs, T. Emrick, T. P. Russell, *Science* **314**, 1107–1110 (2006).
10. S. R. White *et al.*, *Nature* **409**, 794–797 (2001).
11. G. H. Deng, C. M. Tang, F. Y. Li, H. F. Jiang, Y. M. Chen, *Macromolecules* **43**, 1191–1194 (2010).
12. E. Nacu, E. M. Tanaka, *Annu. Rev. Cell Dev. Biol.* **27**, 409–440 (2011).
13. K. Echeverri, E. M. Tanaka, *Semin. Cell Dev. Biol.* **13**, 353–360 (2002).
14. J. I. Morrison, S. Löf, P. He, A. Simon, *J. Cell Biol.* **172**, 433–440 (2006).
15. J. P. Brookes, A. Kumar, *Nat. Rev. Mol. Cell Biol.* **3**, 566–574 (2002).
16. C. Jopling, S. Boue, J. C. Izpisua Belmonte, *Nat. Rev. Mol. Cell Biol.* **12**, 79–89 (2011).
17. S. J. Odelberg, *Anat. Rec. B New Anat.* **287**, 25–35 (2005).
18. J. M. W. Slack, *Trends Cell Biol.* **16**, 273–275 (2006).
19. A. Kumar, C. P. Velloso, Y. Imokawa, J. P. Brookes, *PLoS Biol.* **2**, E218 (2004).

20. C. S. Sheppard, V. R. Kamath, *Polym. Eng. Sci.* **19**, 597–606 (1979).
21. C. E. Hoyle, T. Y. Lee, T. Roper, *J. Polym. Sci. A Polym. Chem.* **42**, 5301–5338 (2004).
22. Y. B. Kim, H. K. Kim, H. C. Choi, J. W. Hong, *J. Appl. Polym. Sci.* **95**, 342–350 (2005).
23. P. Esfandiari *et al.*, *J. Polym. Sci. A Polym. Chem.* **51**, 4261–4266 (2013).
24. T. Tate, *Philos. Mag. Ser. A* **27**, 176–180 (1864).
25. W. D. Harkins, F. E. Brown, *J. Am. Chem. Soc.* **41**, 499–524 (1919).
26. J. L. Lando, H. T. Oakley, *J. Colloid Interface Sci.* **25**, 526–530 (1967).
27. R. J. Wojtecki, M. A. Meador, S. J. Rowan, *Nat. Mater.* **10**, 14–27 (2011).
28. B. A. Beiermann, M. W. Keller, N. R. Sottos, *Smart Mater. Struct.* **18**, 085001 (2009).
29. K. S. Toohey, C. J. Hansen, J. A. Lewis, S. R. White, N. R. Sottos, *Adv. Funct. Mater.* **19**, 1399–1405 (2009).
30. J. E. Mark, Ed., *Polymer Data Handbook* (Oxford Univ. Press, New York, 1999), pp. 656.
31. J. F. Patrick *et al.*, *Adv. Mater.* 10.1002/adma.201400248 (2014).

Acknowledgments: This research has been financially supported by the Air Force Office of Scientific Research (grant FA9550-10-1-0255). We extend our gratitude to the Mechanical Testing Instructional Laboratory (MTIL) and the Beckman Institute for facilities; Y. Fedonina, J. Carlson, A. Komnick, and C. Kirk for assistance with sample fabrication and material synthesis; and G. Milner for test fixture construction.

Supplementary Materials

www.sciencemag.org/content/344/6184/620/suppl/DC1

Materials and Methods

Figs. S1 to S15

Tables S1 to S7

References (32–38)

Movie S1

21 January 2014; accepted 7 April 2014

10.1126/science.1251135

In Situ TEM Observation of a Microcrucible Mechanism of Nanowire Growth

Rebecca Boston,^{1,2} Zoe Schnepf,³ Yoshihiro Nemoto,⁴ Yoshio Sakka,⁴ Simon R. Hall^{1*}

The growth of metal oxide nanowires can proceed via a number of mechanisms such as screw dislocation, vapor-liquid-solid process, or seeded growth. Transmission electron microscopy (TEM) can resolve nanowires but invariably lacks the facility for direct observation of how nanowires form. We used a transmission electron microscope equipped with an in situ heating stage to follow the growth of quaternary metal oxide nanowires. Video-rate imaging revealed barium carbonate nanoparticles diffusing through a porous matrix containing copper and yttrium oxides to subsequently act as catalytic sites for the outgrowth of Y_2BaCuO_5 nanowires on reaching the surface. The results suggest that sites on the rough surface of the porous matrix act as microcrucibles and thus provide insights into the mechanisms that drive metal oxide nanowire growth at high temperatures.

The fabrication of nanowires of functional materials has become an important goal for their application in miniaturized circuits as diodes and transistors, coaxial gates and sensors (1). Fabrication methods such as soft lithography have yielded ternary or more complex metal oxide nanowires (2); however, these types of techniques rely on an underlying substrate that may have a

detrimental effect on the properties of the material. Simple metal oxide nanowires such as ZnO (3) or TiO_2 (4) have been grown with a variety of methods, although the unsupported crystallization of more complex quaternary and quaternary oxide functional materials such as magnetoresistive $\text{La}_{0.67}\text{Ca}_{0.33}\text{MnO}_3$, piezoelectric $\text{PbZr}_{0.52}\text{Ti}_{0.48}\text{O}_3$, and the superconductors $\text{YBa}_2\text{Cu}_3\text{O}_{7-\delta}$ (Y123) and

$\text{Bi}_2\text{Sr}_2\text{Ca}_{n-1}\text{Cu}_n\text{O}_{2n+4+x}$ (BSCCO) is difficult at the nanoscale, owing to the formation of stable impurity phases and/or the lack of a suitable nanoparticulate catalytic seed (1). Wires and whiskers of BSCCO have previously been grown on the macroscale (5, 6), using a rapidly cooled glassy Bi-rich BSCCO precursor seeded with Al_2O_3 powder to provide sites of nucleation and outgrowth. The mechanism for this growth, however, has yet to be fully characterized, and although several processes have been proposed, the microcrucible mechanism is generally the favored one (7).

The microcrucible mechanism is a two-phase growth process that relies on the presence of a liquid and a solid phase. The liquid phase dissolves ions out of a solid matrix, and once supersaturated, growth occurs at the exposed surface of the droplet with the nanowire being extruded from the bulk (5). The microcrucible itself is composed of the solid underlying substrate, which

¹Complex Functional Materials Group, School of Chemistry, University of Bristol, Bristol BS8 1TS, UK. ²Bristol Centre for Functional Nanomaterials, Centre for Nanoscience and Quantum Information, Tyndall Avenue, Bristol BS8 1FD, UK. ³School of Chemistry, University of Birmingham, Birmingham B15 2TT, UK. ⁴National Institute for Materials Science, 1-2-1 Sengen, Tsukuba, Ibaraki 305-0047, Japan.

*Corresponding author. E-mail: simon.hall@bristol.ac.uk

This copy is for your personal, non-commercial use only.

If you wish to distribute this article to others, you can order high-quality copies for your colleagues, clients, or customers by [clicking here](#).

Permission to republish or repurpose articles or portions of articles can be obtained by following the guidelines [here](#).

The following resources related to this article are available online at www.sciencemag.org (this information is current as of March 5, 2015):

Updated information and services, including high-resolution figures, can be found in the online version of this article at:

<http://www.sciencemag.org/content/344/6184/620.full.html>

Supporting Online Material can be found at:

<http://www.sciencemag.org/content/suppl/2014/05/07/344.6184.620.DC1.html>

A list of selected additional articles on the Science Web sites **related to this article** can be found at:

<http://www.sciencemag.org/content/344/6184/620.full.html#related>

This article **cites 33 articles**, 3 of which can be accessed free:

<http://www.sciencemag.org/content/344/6184/620.full.html#ref-list-1>

This article has been **cited by** 1 articles hosted by HighWire Press; see:

<http://www.sciencemag.org/content/344/6184/620.full.html#related-urls>

This article appears in the following **subject collections**:

Materials Science

http://www.sciencemag.org/cgi/collection/mat_sci